Stabilization of Quantum-Confined Anisotropic CsPbI$_3$ Nanoplatelets by Solid-Phase Metal Iodide Crude Reaction for Color-Pure Red Emission

Journal Article

Author(s):
Solari, Simon F.; Wieczorek, Alexander ⬚; Marcato, Tommaso; Wörle, Michael; Krumeich, Frank ⬚; Li, Yen-Ting; Chiu, Yu-Cheng; Siol, Sebastian; Shivarudraiah, Sunil B.; Shih, Chih-Jen

Stabilization of Quantum-Confined Anisotropic CsPbI₃ Nanoplatelets by Solid-Phase Metal Iodide Crude Reaction for Color-Pure Red Emission

Simon F. Solari, Alexander Wieczorek, Tommaso Marcato, Michael Wörle, Frank Krumeich, Yen-Ting Li, Yu-Cheng Chiu, Sebastian Siol,* Sunil B. Shivarudraiah,* and Chih-Jen Shih*

Quantum-confined CsPbI₃ perovskite nanoplatelets (NPLs) are highly desirable for optoelectronic applications owing to their anisotropic electronic properties that substantially boost the light outcoupling efficiency in light-emitting diodes (LEDs). However, the structural instability of the emissive CsPbI₃ phases makes it degrade rapidly to the non-emissive δ-phase under ambient conditions. Here, the study presents a synthetic approach to produce spectrally stable CsPbI₃ nanoplatelets (NPLs) through solid-phase crude reactions with metal iodide powders, MI_2 (M^{2+} = Mn^{2+} or Zn^{2+}). The synthesized NPLs exhibit narrow and color-pure red emission with high photoluminescence (PL) quantum yields (QYs, η_{PL}) of up to 85%. Systematic investigations into the surface chemistry of NPLs reveal that metal iodide treatment stabilizes anisotropic CsPbI₃ NPLs via surface passivation with metal and halide ions, substantially hindering from the formation of non-emissive yellow phase. The anisotropic NPLs display signatures of spontaneous self-assembly in spin-casted films, which yield strong emission anisotropy, with up to 82% of the transition dipoles being horizontally oriented with respect to the substrate, as revealed by the back focal plane (BFP) imaging. The results presented here shed light on solid-phase approaches for the preparation of quantum-confined nanocrystals (NCs) with desirable geometry, which boost the light outcoupling efficiency in LEDs.

1. Introduction

Colloidal perovskite nanocrystals (PeNCs) have emerged as a novel class of nanomaterials with exceptional optical and electronic properties, sparking immense interest in light-emitting diodes (LEDs), solar cells, lasers, and photodetectors.[1–8] The emission wavelengths (λ_{PL}) and the absorption properties of PeNCs can be easily tuned over the whole visible spectra by varying the composition or size-dependent quantum confinement.[9–11] Moreover, owing to their inherent softness and ionic lattice, perovskite materials offer controllable manipulation of shape and size across various dimensions, including quantum dots, nanorods, nanoplatelets, and nanosheets.[12–16] Of the various nanostructures, nanoplatelets (NPLs) uniquely exhibit anisotropic emission, a characteristic that enhances light extraction efficiency and directionality, thereby significantly improving device performance.[17–21] Green-emitting perovskite NPLs have

S. F. Solari, T. Marcato, S. B. Shivarudraiah, C.-J. Shih
Institute for Chemical and Bioengineering
ETH Zürich
Zürich 8093, Switzerland
E-mail: sshivarudrai@ethz.ch; chih-jen.shih@chem.ethz.ch
A. Wieczorek, S. Siol
Laboratory for Surface Science and Coating Technologies
Empa – Swiss Federal Laboratories for Materials Science and Technology
Dübendorf 8600, Switzerland
E-mail: sebastian.siol@empa.ch

M. Wörle, F. Krumeich
Laboratory of Inorganic Chemistry
ETH Zürich
Zürich 8093, Switzerland
Y.-T. Li, Y.-C. Chiu
Department of Chemical Engineering
National Taiwan University of Science and Technology
Taipei 10607, Taiwan
Y.-T. Li
National Synchrotron Radiation Research Center
Hsinchu 30076, Taiwan
Y.-C. Chiu
Advanced Research Center for Green Materials Science and Technology
National Taiwan University
Taipei 10617, Taiwan

**ADVANCED
SCIENCE NEWS**

www.advancedsciencenews.com

**ADVANCED
OPTICAL
MATERIALS**

www.advopticalmat.de

demonstrated superior spectral stability, color purity, and tunable transition dipole moment (TDM) orientation in PL for enhancing intrinsic light outcoupling efficiency in thin-film LEDs.[22–24] However, the emission spectra for perovskite red emitters, such as $CsPbI_3$ NCs, typically peak beyond 640 nm, which does not comply with that for the red primary (620–635 nm) in recommendation (Rec.) 2020 standard.[25] Although it is straightforward to reach the emission wavelength through halide mixing (Br^- and I^-),[26–28] the mixed-halide PeNCs suffer from halide segregation under electrical stress,[29–31] which leads to reduced spectral stability and broadening of the electroluminescence (EL) spectra,[26,32] considerably compromising the device performance. In this regard, it is highly desirable to synthesize stable and pure-red-emitting $CsPbI_3$ NCs with controlled quantum confinement.

There are a number of reports in the literature demonstrating the pure-red-emitting quantum-confined $CsPbI_3$ NCs.[25,33–37] However, although quantum-confined $CsPbI_3$ NCs hold promise for optoelectronic applications, they face instability issues, including phase transitions and morphological transformations.[38,39] Indeed, the optically active $CsPbI_3$ perovskite black phase (α, β, and γ) is metastable relative to its non-perovskite yellow phase (δ) at room temperature.[40] As a result, quantum-confined $CsPbI_3$ NCs with a cubic α-phase tend to degrade under ambient conditions to the non-perovskite δ-phase, thereby diminishing the optical properties and colloidal stability.[38,41–48] In addition, the synthesis of quantum-confined $CsPbI_3$ NCs typically involves complex protocols conducted under inert atmospheres and at elevated temperatures, potentially impeding progress toward commercialization.[33–35,49] Hot-injection synthesis of pure-red-emitting $CsPbI_3$ NPLs is even more challenging because the rapid crystallization kinetics make shape modulation difficult. Recently, the ligand-assisted reprecipitation (LARP) approach, commonly employed for synthesizing PeNCs under ambient conditions, has also been applied to the synthesis of $CsPbI_3$ NCs and NPLs.[25,50,51] However, the quantum-confined $CsPbI_3$ NPLs exhibited poor spectral stability, characterized by broadened PL peaks, diminished color purity, and loss of anisotropic emission.[50] Numerous approaches have been developed to stabilize the red-emitting $CsPbI_3$ NCs and NPLs, including surface passivation,[52–54] ligand engineering,[41,55] and presynthetic metal doping.[56] Nevertheless, there is a lack of synthetic strategies to stabilize the pure-red-emitting $CsPbI_3$ NPLs prepared by LARP, including their oriented thin films showing anisotropic emission, which is highly desirable for LED applications.

In this work, we present a facile synthetic approach to stabilize quantum-confined $CsPbI_3$ NPLs by solid-phase passivation with metal iodide powders, MI_2 (M = Mn^{2+} or Zn^{2+}). The metal-doped NPLs exhibit outstanding optical properties, including high η_{PL}, narrowband emission, and notably, exceptional spectral stability compared to as-prepared NPLs. Additionally, the emission spectra centered at 627–628 nm with CIE color coordinates of (0.677, 0.323) and (0.680, 0.320) for Mn:$CsPbI_3$ and Zn:$CsPbI_3$ NPLs, respectively, nicely meet the Rec. 2020 standard. The treatment with solid metal iodides effectively prevents the phase transition to the non-perovskite δ-phase, in contrast to the undoped NPLs, which experience spectral instability, subsequent loss of anisotropic morphology, and degradation, as confirmed by opti-

cal and structural characterization. Employing an internal charge reference method in X-ray photoelectron spectroscopy (XPS), we observed changes in electron density at the Pb-site of the lattice upon doping, suggesting that the halide vacancies are passivated. The doped $CsPbI_3$ NPLs preserve their anisotropic platelet shape and exhibit preferential face-on assembly in solid thin films. We conducted a comprehensive analysis of the orientational ordering of the resulting solids using grazing incidence wide-angle X-ray scattering (GIWAXS) and back focal plane (BFP) imaging. This investigation unveiled a markedly anisotropic PL emission, with up to 82% of the transition dipoles that are horizontally oriented with respect to the substrate.

2. Results and Discussion

We synthesized the $CsPbI_3$ NPLs dispersed in toluene using the ligand-assisted reprecipitation (LARP) protocol.[57] In short, PbI_2 was dissolved in toluene containing oleic acid (OLAc), oleylamine (OLAm), and lecithin,[58] followed by adding the Cs-oleate precursors and stirring for one hour at room temperature and ambient conditions. During the synthesis of $CsPbI_3$ NPLs, the color of the reaction mixture turned from orange to red, and different quantum-confined species could be identified by absorption and PL spectroscopy (Figure S1, Supporting Information). The colloidal NPLs then underwent a solid-phase reaction by directly mixing with solid powders of MI_2 (M = Mn^{2+} or Zn^{2+}) at room temperature and ambient conditions for up to 15 hours, yielding metal-doped $CsPbI_3$ NPLs.[59] Unreacted precursors and excess surfactants were removed by anti-solvent purification, followed by redispersion of the NPLs in toluene. **Figure 1a** presents a schematic diagram for the synthetic process.

The metal iodide salts were chosen to prevent the NPLs from undesirable halide exchange reactions.[60] After the purification of the colloidal perovskite NPLs, Mn and Zn contents were successfully detected in the metal-doped perovskites by the semi-quantitative energy-dispersive X-ray spectroscopy (EDXS) analysis (Figure S2, Supporting Information). Specifically, EDXS results revealed a small fraction of guest metals (≈3 at.% Mn and ≈6 at.% Zn) in the perovskite structures. Interestingly, the iodine content slightly increased from ≈60 at.% up to ≈65 at.% upon crude solution metal iodide treatment (Figure S2b, Supporting Information).

Absorption and PL spectra of the parent and metal-doped perovskite NPLs are shown in Figure 1b. The metal-doped $CsPbI_3$ NPLs exhibit $\lambda_{PL} = 628$ nm for Mn:$CsPbI_3$ and $\lambda_{PL} = 627$ nm for Zn:$CsPbI_3$ NPLs, respectively, as compared to undoped $CsPbI_3$ NPLs ($\lambda_{PL} = 639$ nm). Metal doping results in high photoluminescence quantum yields, η_{PL}, reaching up to 85%. The related absorption spectra revealed the quantum-confined nature of the NPLs, with sharp excitonic absorption features observed across all samples. Furthermore, the full width at half maximum (FWHM) of the PL emission peak was further narrowed from 42 nm for the undoped $CsPbI_3$ NPLs down to 37 nm for the metal-doped $CsPbI_3$ NPLs. The blueshift of the optical bandgap could be either attributed to the lattice contraction of the perovskite unit cell upon replacing Pb^{2+} by the smaller divalent cations Mn^{2+} and Zn^{2+} or a small degree of size reduction effects in quantum-confined systems upon metal iodide treatment.[11,61–65]

**ADVANCED
SCIENCE NEWS**

www.advancedsciencenews.com

**ADVANCED
OPTICAL
MATERIALS**
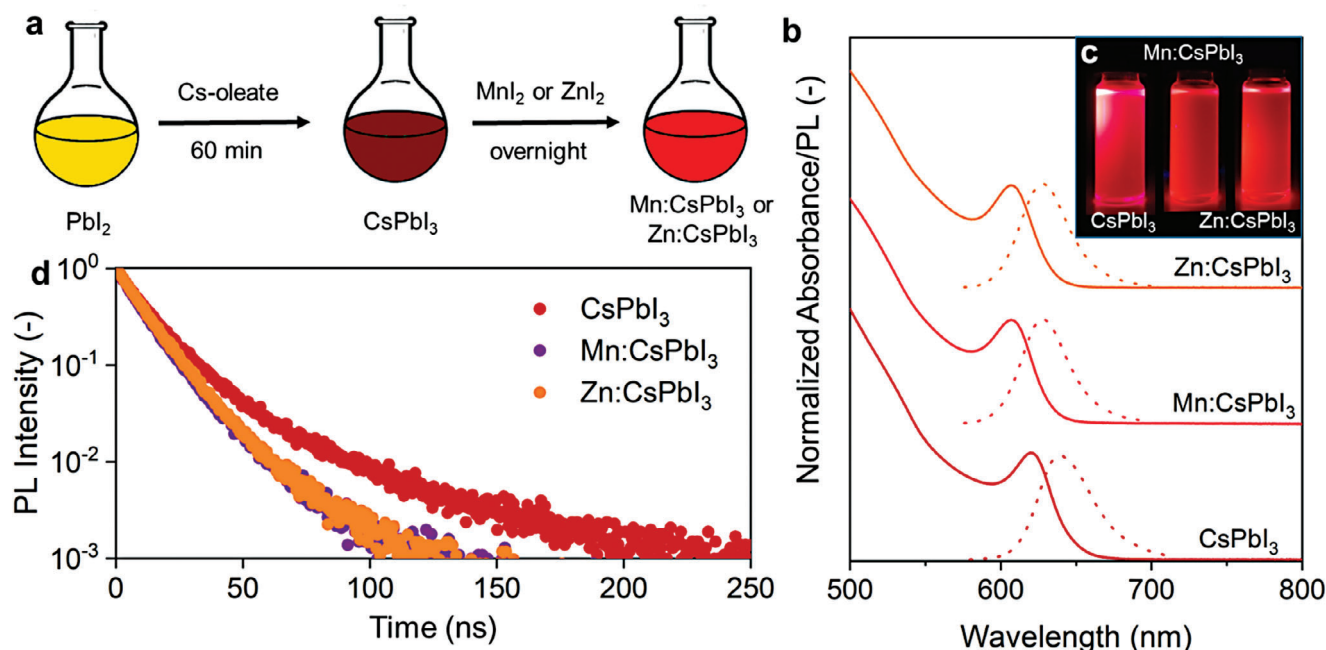
www.advopticalmat.de

Figure 1. Synthesis and optical characterization of quantum-confined, metal-doped CsPbI₃ NPLs. a) Schematic diagram for the synthesis of CsPbI₃ and metal-doped CsPbI₃ NPLs. b) Absorption (solid line) and PL (dashed line) spectra for the as-synthesized CsPbI₃ NPLs. c) Representative photographs of synthesized colloidal solutions under UV excitation. d) Comparison of PL lifetimes for bare CsPbI₃ NPLs and metal-doped NPLs.

The PL color purity for the CsPbI₃ NPLs remain intact after doping, as demonstrated in Figure 1c. Remarkably, the red-emitting perovskite NPLs exhibit CIE color coordinates of (0.677, 0.323) for Mn:CsPbI₃ and (0.680, 0.320) for Zn:CsPbI₃ NPLs, within the Rec. 2020 standard for color-pure red primary (Figure S3, Supporting Information). The PL lifetimes of the parent CsPbI₃ NPLs and the metal-doped NPLs are presented in Figure 1d, whereas their carrier lifetimes are shown in Table S1 (Supporting Information). Interestingly, a shortening of the average PL lifetime, τ_{avg}, was observed from 21.7 ± 1.2 ns for the parent NPLs down to 13.1 ± 0.4 ns for the Mn:CsPbI₃ and 13.2 ± 0.3 ns for the Zn:CsPbI₃ NPLs, respectively, which has been observed in the literature that the intrinsic optical properties of the CsPbI₃ NPLs are affected by the incorporation of Mn²⁺ and Zn²⁺.[59,61,66,67]

More specifically, the enhanced photophysical properties for the metal-treated NPLs, namely shortened radiative lifetime accompanied by enhanced η_{PL}, could be attributed to an increased charge carrier localization through lattice periodicity breaking resulting from the metal dopants. The scenario results in an increased overlap for the electron and hole wavefunctions, thereby considerably increasing the radiative recombination rate. Additionally, the charges become localized around the metal dopant and are therefore less likely to diffuse to remaining trap sites, which would otherwise promote non-radiative recombination processes.[67,68]

Figure 2a compares the absorption spectra for our synthesized NPLs dispersed in solution recorded spanning 360 minutes. For undoped CsPbI₃ NPLs, we observed a relative intensity reduction of the sharp excitonic peak and the emergence of an additional weak absorption shoulder ≈680 nm. We carried out a longer-term stability test (Figure S4, Supporting Information),

revealing a redshift and a reduction of the excitonic absorption feature, suggesting the loss of quantum-confinement over a storage time of 10 days for the parent CsPbI₃ NPLs. Furthermore, a strong absorption peak at ≈380 nm is detected after 10 days, which could be attributed to an optical transition of the non-emissive δ-phase of CsPbI₃.[69] The PL spectra are consistent with the absorption spectra. Notably, untreated CsPbI₃ NPLs exhibit substantial emission broadening and a secondary PL peak at λ_{PL} = 689 nm, exceeding the spectral range for color-pure red emitters (Figure 2b). The PL intensity of undoped CsPbI₃ NPLs dropped significantly (decreased η_{PL}) following the degradation to the non-emissive yellow phase (Figure S4, Supporting Information).[55,70]

Conversely, the spectra remained stable for the metal-doped NPLs. The PL properties of Mn:CsPbI₃ and Zn:CsPbI₃ NPLs remain unchanged in 360 min, exhibiting enhanced spectral stability following crude solution metal iodide treatment. In particular, the excitonic absorption feature was preserved for a longer time in the metal-doped NPLs. In the case of Zn:CsPbI₃ NPLs, an optical transition related to the δ-phase could be observed after a few days, suggesting a partial transition from the black phase to the yellow phase, whereas the PL peak position of the metal-doped NPLs could be preserved for a few days.

We further examined the UV stability of the metal-treated NPLs by continuously illuminating them with UV light. The metal-doped samples show no peak shift of λ_{PL} and maintain their high η_{PL}, whereas the undoped CsPbI₃ samples exhibit a significant peak shift and a reduction in η_{PL} to <20% after 240 min of continuous irradiation (Figure S5, Supporting Information). Overall, the improved spectral and colloidal stability of the metal-doped NPLs over the CsPbI₃ NPLs could result from an inhibition of the NPL fusion, following the passivation of trap
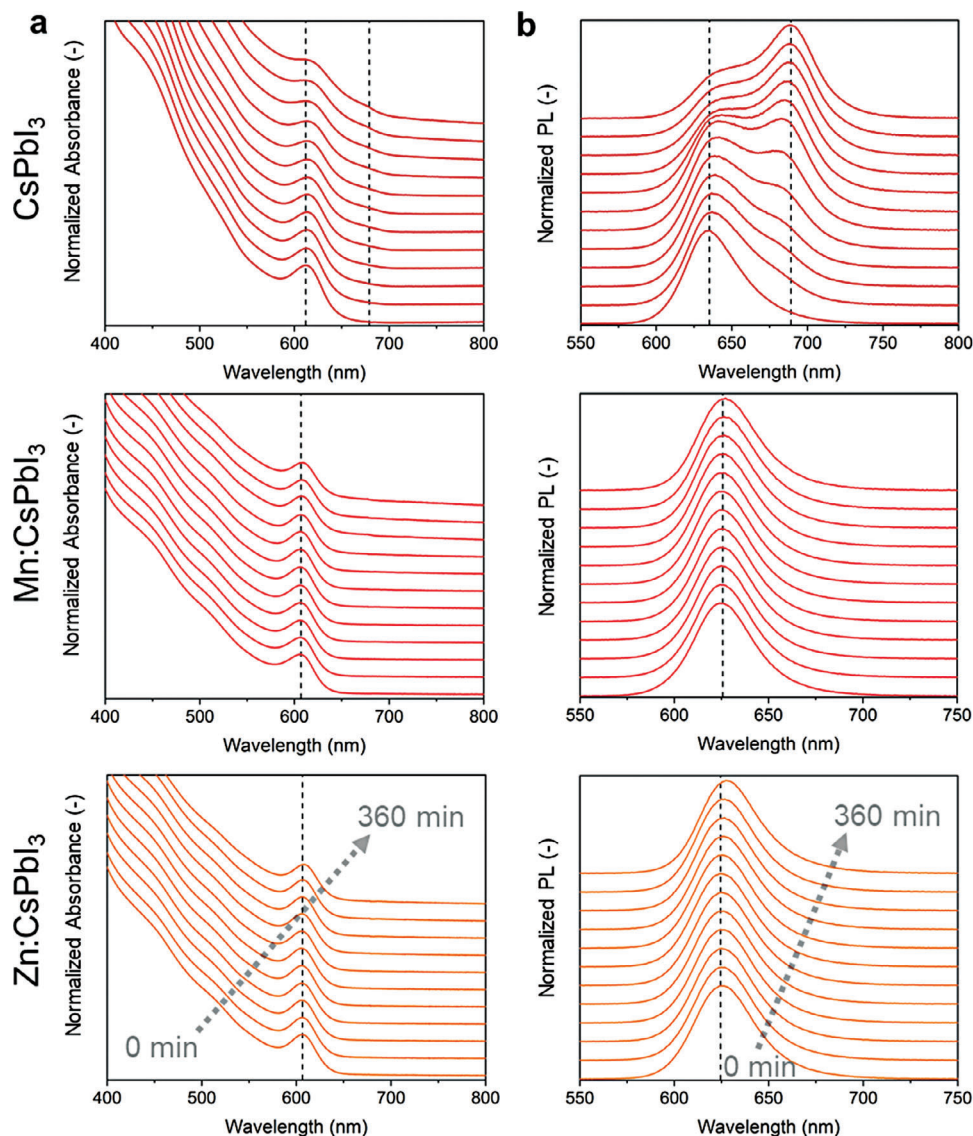
**ADVANCED
SCIENCE NEWS**

www.advancedsciencenews.com

**ADVANCED
OPTICAL
MATERIALS**

www.advopticalmat.de

Figure 2. Comparison of spectral stability of undoped and doped $CsPbI_3$ NPLs. a) Time-dependent absorption and b) PL spectra for the diluted solutions reveal that solid-phase metal doping effectively stabilizes the spectral stability of the quantum-confined perovskite red emitters.

states on the NPL surfaces by the additional guest ions incorporated during the crude solution metal iodide treatment.[55,71–73]

We carried out X-ray diffraction (XRD) to gain more insight into the crystallographic nature of the phase transition. Due to the nanoscale nature of these materials,[74] a broadening of diffraction peaks for the black phase results in considerable overlaps, rendering an unambiguous assignment of crystallography difficult. Therefore, the measured X-ray diffractograms for fresh and aged perovskite samples were qualitatively compared with the calculated powder patterns of the two black phases (cubic α-phase, ICSD 161481, and orthorhombic γ-phase, ICSD 32310) and the yellow phase (orthorhombic δ-phase, ICSD 250744). This comparison is made under the assumption of an average crystallite size of 10 nm for the nanoscale materials and 3 µm for the δ-phase crystals, as illustrated in Figure S6 (Supporting Information).

Figure 3a–c compare the measured and calculated XRD patterns (α, γ, their 1:1 sum, and δ) for $CsPbI_3$ (Figure 3a) and metal-doped NPLs (Figure 3b,c). From a first point of view, we could assign the main diffraction peaks for $CsPbI_3$ NPLs at $2\theta = 14.4°$ and $2\theta = 28.7°$ to (100) and (200) planes the cubic α-phase.[33,75] However, the splitting of the peak belonging to the (200) lattice plane suggests a mixed cubic (α) and orthorhombic (γ) phase,[76] nicely agreeing with the calculated (1:1) mixed pattern. Due to the nanoscale broadening, a reduction of symmetry elements upon distortion of the $[PbI_6]^{4-}$ octahedral, which results in peak splits of the simple cubic pattern, is not observed. Upon aging of the colloidal $CsPbI_3$ NPLs, a phase transition from the mixed black phase to the yellow phase was confirmed,[41] matching the calculated δ-phase pattern.

At the first glance, no signs of transition to the yellow phase could be observed in the case of the Mn:$CsPbI_3$ NPLs, indicating
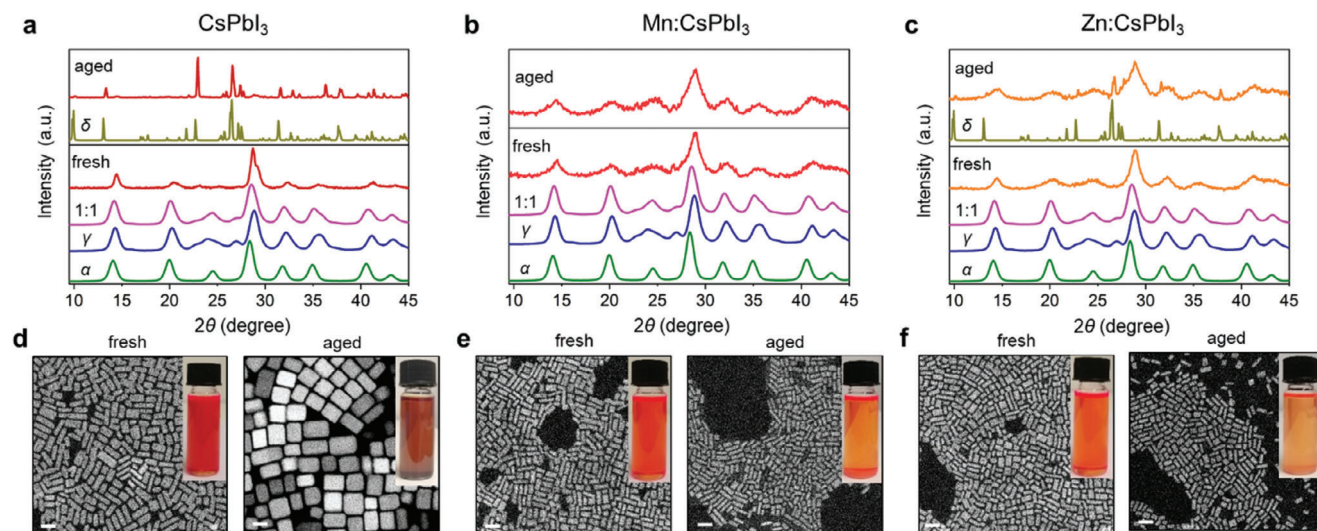
**ADVANCED
SCIENCE NEWS**

www.advancedsciencenews.com

**ADVANCED
OPTICAL
MATERIALS**

www.advopticalmat.de

Figure 3. Crystallography and morphology for the fresh and aged NPLs. Measured XRD patterns for a) $CsPbI_3$, b) $Mn:CsPbI_3$, and c) $Zn:CsPbI_3$ NPLs (fresh and aged), in comparison with the powder XRD patterns for the black cubic (α, ICSD 161481), orthorhombic (γ, ICSD 32310), their 1:1 sum, and the yellow orthorhombic (δ, ICSD 250744) phases. STEM images and photographs for the fresh and aged colloidal dispersion of d) parent $CsPbI_3$, e) $Mn:CsPbI_3$, and f) $Zn:CsPbI_3$ nanostructures. Scale bars: 20 nm.

improved stability upon MnI_2 solid-state treatment. On the other hand, in addition to the broad peaks arising from the nanomaterial, narrow peaks were already found in the case of the aged $Zn:CsPbI_3$ NPLs, suggesting a partial transition from the emissive black phase to the non-emissive yellow phase, which is consistent with the appearance of the absorption signal that can be assigned to the δ-phase. (Figure S4a, Supporting Information). Although the main diffraction peaks for the metal-doped samples are slightly shifted toward higher angles, which could result from contraction of the perovskite lattice,[62,77] one could not exclude the scenario of zero point shift due to the broad and overlapping nature of these peaks.[74]

The scanning transmission electron microscope (STEM) images (Figure 3d–f) reveal anisotropic shape of the as-prepared NPLs. The statistical size analysis shows that the average NPL width was reduced from ≈6 to ≈4 nm upon metal doping, whereas the average length remained unchanged at ≈13 nm (Figure S7, Supporting Information). The size reduction in one spatial direction of quantum-confined systems could explain the blueshift of the optical bandgap upon the crude solution treatment (Figure 1b).[9,64,78] Remarkably, STEM images of an aged colloidal $CsPbI_3$ dispersion experienced a morphological transformation from quantum-confined NPLs to nanocubes with increased dimensionality. This transformation aligns with the observed color shift in the colloidal solution and previously noted spectral instability, indicating a loss of quantum confinement and significant redshifts in both absorption and PL spectra (Figure 2; Figure S4, Supporting Information). The emergence of the PL emission peak at $\lambda_{PL} = 689$ nm in the undoped samples (Figure 2b) results from the morphological transformation via the Ostwald ripening mechanism, where smaller NCs of high surface energy coalesce into larger ones with reduced surface energy. The diffusion of halide vacancies and ligand desorption create surface active sites that drive the growth.[79,80] The addition of excess metal and halide ions not only passivates the nanocrys-

tal surfaces but also changes the thermodynamic equilibrium of the parent solution,[9] substantially stabilizing the NPLs kinetically. Consequently, the doped samples show higher morphological stability without PL emission peak shifts.

On the other hand, the shape and average size of the $Mn:CsPbI_3$ and $Zn:CsPbI_3$ NPLs were preserved upon aging (Figure S8, Supporting Information). The observed fusion or aggregation processes of the parent $CsPbI_3$ NPLs to bigger nanocubes could result from an iodine inadequacy and defects on the NPL surface.[81–83] The enhanced phase stability of the metal-doped samples may arise from the lower Shannon ionic radii of Mn^{2+} and Zn^{2+} compared to Pb^{2+} which would result in a more ideal Goldschmidt factor.[84] Indeed, the lower value for Mn^{2+} (0.67 Å) compared to Zn^{2+} (0.74 Å)[85] could explain the superior phase stability upon MnI_2 treatment.

We further carried out X-ray photoelectron spectroscopy (XPS) to examine chemical states at the NC surface (Figure S9, Supporting Information). Note that for semiconductors and insulators especially, binding energy (E_b) shifts of several eV could arise from charging effects in XPS. Charge referencing based on the C 1s feature of adventitious carbon is often employed, but may still induce errors of up to 2 eV.[86] For this reason internal charge referencing concepts have recently been more widely applied for semiconducting and insulating samples.[87–90] By using internal charge references, i.e., the energetic distance between features, rather than their absolute binding energies, one can resolve even small binding energy shifts reliably and consequently probe even minor changes of the local chemical environment of the probed atoms. To probe differences in the local chemical environment in $CsPbI_3$ NPLs upon doping, analysis based on the E_b distance of the Pb $4f_{7/2}$ and I $3d_{5/2}$ core level emission is performed (**Figure 4a**). For validation of the results, sample statistics were conducted (Figure 4b). In addition, additional experiments including energy referencing at different probing depths were performed to exclude vertical charging
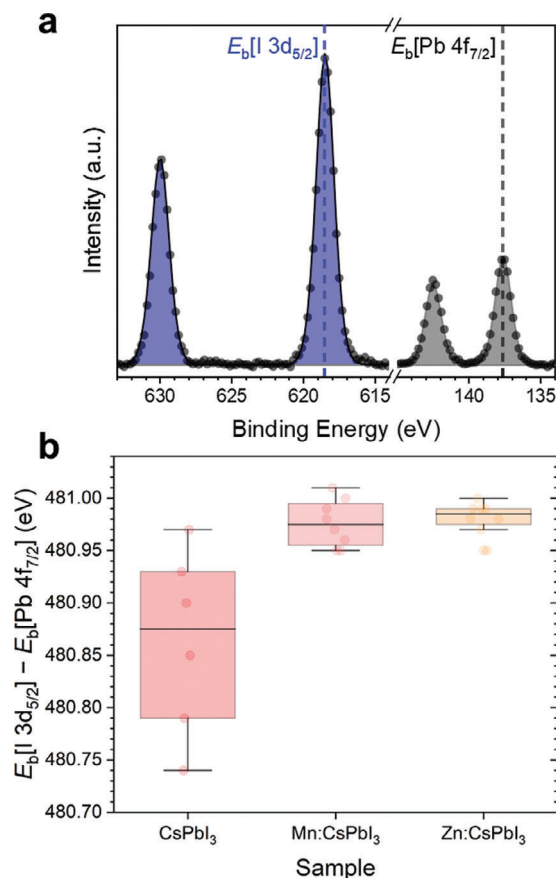
Figure 4. a) Concept of internal binding energy (E_b) referencing based on Pb $4f_{7/2}$ (grey) and I $3d_{5/2}$ (blue) features for improved charge referencing. b) Result of statistical XPS analysis obtained from two sample batches and multiple sample spots. The statistical approach allows to verify the significance of the observed minor relative shifts. Furthermore, a relatively higher spread of the shifts was determined for the parent $CsPbI_3$, indicating inhomogeneity on the surface.

effects, which may add a degree of uncertainty to the chemical state analysis, even with internal charge referencing (Figure S10, Supporting Information).[91,92] Based on these results, the metal-doped $CsPbI_3$ NPLs exhibited no overlap of the determined relative Pb chemical shift within the interquartile range. Furthermore, the relative shift of the Pb $4f_{7/2}$ feature compared to I $3d_{5/2}$ toward lower E_b values indicates a change in the electron distribution between the Pb- and I-sites compared to the halide site for treated samples. This minor shift of 0.1 eV may arise from iodide passivation effects or B-site doping at the NPL surface upon MI_2 treatment. In comparison to EDXS analysis, which is less surface-sensitive than XPS,[93,94] the quantities of Mn and Zn detected on the surface were either below or near the detection limit of 1–2 at.% (Figure S11, Supporting Information). This indicates that these ions are predominantly situated within the core of the nanomaterials, aligning with the higher concentrations of metals identified by the EDXS analysis (Figure S2b, Supporting Information).

Strikingly, the distinctively reduced spread in the relative E_b shift observed in the metal-doped samples suggests an enhanced stability in the surface chemistry of NPLs. This increased stability

for both metal iodide treatments may play a role in inhibiting the fusion of quantum-confined NPLs into redshifted nanocubes of larger sizes, as evidenced by the morphological transformation of undoped $CsPbI_3$ NPLs (Figure 3d). Furthermore, it could contribute to preventing the eventual degradation of optically active perovskite species into the yellow δ-phase.[55,70] Overall, these results highlight how the more robust internal charge referencing allows to probe minor changes in the Pb and I chemical states.

In light of the high η_{PL} and spectral stability of our metal-doped NPLs, we further examined their NPL solid films. Recent studies have highlighted the significance of characterizing the orientational distribution of nanocrystal solids, particularly in the context of their optoelectronic properties.[22,24,95] Indeed, the reduction of disorder in NC packing has a direct impact on promoting internanocrystal charge and exciton transport due to increased transfer integrals and in enhancing light outcoupling. Furthermore, the dynamics of solvent evaporation has been identified as a crucial factor controlling NPL self-assembly in either face-on or edge-on configurations.[96] We directly prepared the NPL solid thin films by either spin coating or drop casting on glass substrates, followed by analyzing the thin-film crystallographic and optical properties.

Figure 5a,e present the grazing incidence wide-angle X-ray spectroscopy (GIWAXS) patterns used for analyzing NPL packing orientation and disorder. The pole figures were constructed by obtaining polar linecuts at the (100) Bragg peak radial position. Both spin-coated NPL samples exhibit strong Laue spots rather than the Debye-Scherrer rings, suggesting well-defined NPL packing ordering. In contrast, the drop-casted films displayed the flat pole figure characteristic of isotropic orientation (Figure 5b,f). The presence of the (100) Bragg peak ($q \approx$ 1 Å^{-1}) along the q_z axis confirmed the face-on configuration of the NPLs. The thin-film orientational characteristics are consistent with the signatures of NPL solids reported in recent literature.[22,24]

We further examined the PL angular emission patterns using the back focal plane (BFP) imaging.[97] This technique effectively generates the spatial Fourier transform of its front focal plane image on its back focal plane, revealing the radiation pattern of an emitter. Different points in the BFP image represent emission angles in the sample plane and linecuts are effectively angle-dependent PL profiles. The average orientation of transition dipole moment (TDM) can therefore be determined by fitting the horizontal p-polarized BFP linecut, which informs radiation resulting from both in-plane and out-of-plane dipoles. Figure 5c,g show the experimental BFP images of the two metal-doped NPL spic-coated films. We used a high-NA oil-immersion objective to collect radiation with the wave vector, $k_{\parallel}/k_0$, where k_0 is the wave vector in air, up to 1.3. Qualitatively speaking, at a given p-polarized linecut profile, a higher ratio for the radiation emitted at the zero angle, $k_{\parallel}/k_0 = 0$ to that at the critical angle, $k_{\parallel}/k_0 = 1$, suggest that the TDM is more horizontally oriented. Figure 5d,h present the p-polarized (p-pol.) and s-polarized (s-pol.) linecuts and their theoretical fittings within $-1.1 < k_{\parallel}/k_0 <$ 1.1, revealing that both $Mn:CsPbI_3$ and $Zn:CsPbI_3$ NPLs exhibit a substantial contribution of in-plane dipoles, with the horizontal dipole ratio values, Θ_{IP}, of 0.82 and 0.75, respectively. A higher Θ_{IP} value >0.67 can substantially enhance the light outcoupling efficiency in their LEDs.

ADVANCED
SCIENCE NEWS

www.advancedsciencenews.com

ADVANCED
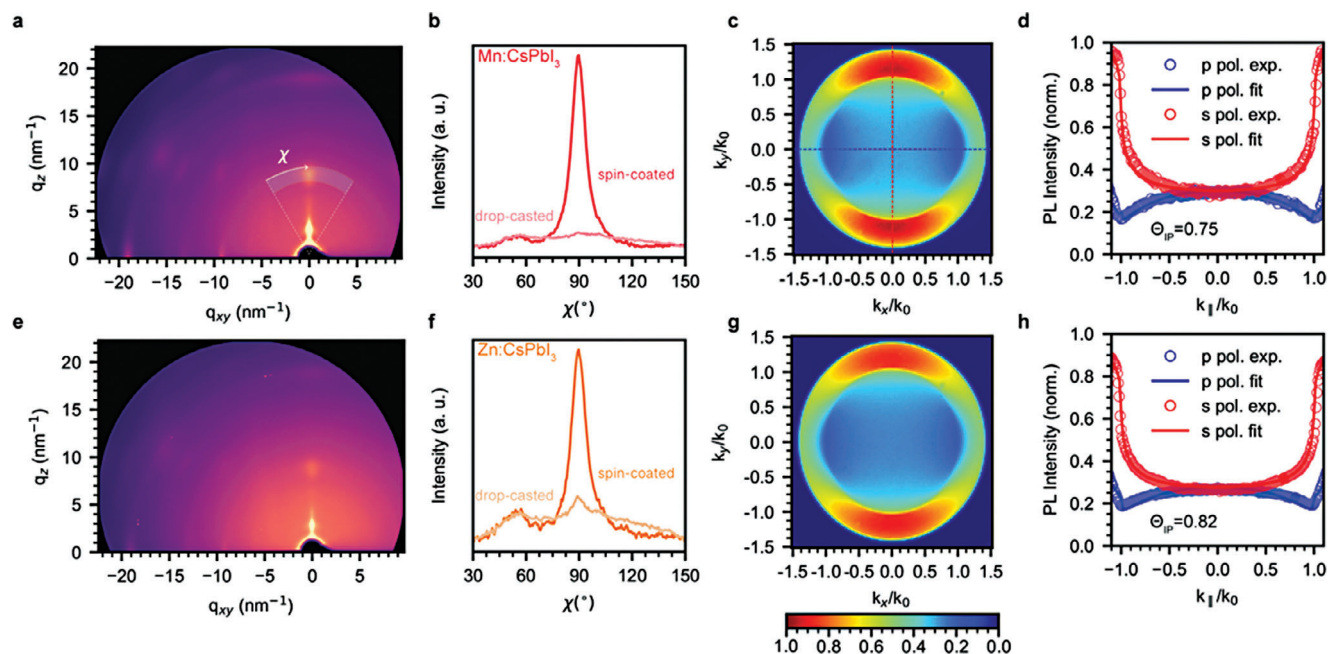**OPTICAL**
MATERIALS

www.advopticalmat.de

Figure 5. a,e) GIWAXS diffractograms for the spin-coated NPL films. b,f) Extracted orientation distribution of spin-coated and drop-casted NC films showing signature of preferential face-on packing orientation in the spin-coated films. c,g) The back focal plane images for Mn:CsPbI$_3$ and Zn:CsPbI$_3$ NPL thin films. d,h) *p*-polarized and *s*-polarized BFP linecuts in comparison with the theoretical fittings for the estimation of transition dipole moment orientation.

3. Conclusion

In summary, we present a solid-phase synthetic approach for preparing metal-doped CsPbI$_3$ NPLs with enhanced colloidal and spectral stability. The quantum-confined NPLs exhibit color-pure emission fulfilling the color coordinates of red primary in the CIE chart. XRD characterizations revealed a phase mixture of the optically active black phase (α and γ), which transforms to the non-emissive δ-phase upon aging of the parent CsPbI$_3$ NPLs, whereas the phase transition could be inhibited upon metal iodide treatment. Together with EDXS and XPS evidence, we conclude that the guest metal atoms not only incorporate into the NPL lattice but also passivate the NPL surface. The spin-coated NPL thin films have face-on orientation, thereby yielding anisotropic PL emission with a high ratio of horizontally oriented transition dipoles. Together with their QYs, we believe the NPLs are promising for future LED applications overcoming the light outcoupling efficiency limit.

Supporting Information

Supporting Information is available from the Wiley Online Library or from the author.

Conflict of Interest

The authors declare no conflict of interest.

Data Availability Statement

The data that support the findings of this study are available from the corresponding author upon reasonable request.

[1] L. Protesescu, S. Yakunin, M. I. Bodnarchuk, F. Krieg, R. Caputo, C. H. Hendon, R. X. Yang, A. Walsh, M. V. Kovalenko, *Nano Lett.* **2015**, *15*, 3692.

[2] F. Krieg, S. T. Ochsenbein, S. Yakunin, S. ten Brinck, P. Aellen, A. Süess, B. Clerc, D. Guggisberg, O. Nazarenko, Y. Shynkarenko, S. Kumar, C.-J. Shih, I. Infante, M. V. Kovalenko, *ACS Energy Lett.* **2018**, *3*, 641.

[3] Q. A. Akkerman, G. Rainò, M. V. Kovalenko, L. Manna, *Nat. Mater.* **2018**, *17*, 394.

[4] Y.-H. Kim, S. Kim, A. Kakekhani, J. Park, J. Park, Y.-H. Lee, H. Xu, S. Nagane, R. B. Wexler, D.-H. Kim, S. H. Jo, L. Martínez-Sarti, P. Tan, A. Sadhanala, G.-S. Park, Y.-W. Kim, B. Hu, H. J. Bolink, S. Yoo, R. H. Friend, A. M. Rappe, T.-W. Lee, *Nat. Photonics* **2021**, *15*, 148.

[5] S. F. Solari, S. Kumar, J. Jagielski, C.-J. Shih, *J. Soc. Inf. Disp.* **2019**, *27*, 667.

[6] T. Chiba, Y. Hayashi, H. Ebe, K. Hoshi, J. Sato, S. Sato, Y.-J. Pu, S. Ohisa, J. Kido, *Nat. Photonics* **2018**, *12*, 681.

[7] A. Swarnkar, A. R. Marshall, E. M. Sanehira, B. D. Chernomordik, D. T. Moore, J. A. Christians, T. Chakrabarti, J. M. Luther, *Science* **2016**, *354*, 92.

[8] Q. Zhao, A. Hazarika, X. Chen, S. P. Harvey, B. W. Larson, G. R. Teeter, J. Liu, T. Song, C. Xiao, L. Shaw, M. Zhang, G. Li, M. C. Beard, J. M. Luther, *Nat. Commun.* **2019**, *10*, 2842.

[9] Y. Dong, T. Qiao, D. Kim, D. Parobek, D. Rossi, D. H. Son, *Nano Lett.* **2018**, *18*, 3716.

[10] S. F. Solari, S. Kumar, J. Jagielski, N. M. Kubo, F. Krumeich, C.-J. Shih, *J. Mater. Chem. C* **2021**, *9*, 5771.

[11] Q. Zhao, A. Hazarika, L. T. Schelhas, J. Liu, E. A. Gaulding, G. Li, M. Zhang, M. F. Toney, P. C. Sercel, J. M. Luther, *ACS Energy Lett.* **2020**, *5*, 238.

[12] Y. Zhang, J. Liu, Z. Wang, Y. Xue, Q. Ou, L. Polavarapu, J. Zheng, X. Qi, Q. Bao, *Chem. Commun.* **2016**, *52*, 13637.

[13] H. Yang, Y. Zhang, J. Pan, J. Yin, O. M. Bakr, O. F. Mohammed, *Chem. Mater.* **2017**, *29*, 8978.

[14] M. Chen, Y. Zou, L. Wu, Q. Pan, D. Yang, H. Hu, Y. Tan, Q. Zhong, Y. Xu, H. Liu, B. Sun, Q. Zhang, *Adv. Funct. Mater.* **2017**, *27*, 1701121.

[15] Q. A. Akkerman, S. G. Motti, A. R. Srimath Kandada, E. Mosconi, V. D'Innocenzo, G. Bertoni, S. Marras, B. A. Kamino, L. Miranda, F. De Angelis, A. Petrozza, M. Prato, L. Manna, *J. Am. Chem. Soc.* **2016**, *138*, 1010.

[16] J. Jagielski, S. F. Solari, L. Jordan, D. Scullion, B. Blülle, Y.-T. Li, F. Krumeich, Y.-C. Chiu, B. Ruhstaller, E. J. G. Santos, C.-J. Shih, *Nat. Commun.* **2020**, *11*, 387.

[17] R. Scott, J. Heckmann, A. V. Prudnikau, A. Antanovich, A. Mikhailov, N. Owschimikow, M. Artemyev, J. I. Climente, U. Woggon, N. B. Grosse, A. W. Achtstein, *Nat. Nanotechnol.* **2017**, *12*, 1155.

[18] J. Cui, Y. Liu, Y. Deng, C. Lin, Z. Fang, C. Xiang, P. Bai, K. Du, X. Zuo, K. Wen, S. Gong, H. He, Z. Ye, Y. Gao, H. Tian, B. Zhao, J. Wang, Y. Jin, *Sci. Adv.* **2021**, *7*, eabg8458.

[19] J. Shamsi, P. Rastogi, V. Caligiuri, A. L. Abdelhady, D. Spirito, L. Manna, R. Krahne, *ACS Nano* **2017**, *11*, 10206.

[20] T. Marcato, F. Krumeich, C.-J. Shih, *ACS Nano* **2022**, *16*, 18459.

[21] J. Ye, A. Ren, L. Dai, T. K. Baikie, R. Guo, D. Pal, S. Gorgon, J. E. Heger, J. Huang, Y. Sun, R. Arul, G. Grimaldi, K. Zhang, J. Shamsi, Y.-T. Huang, H. Wang, J. Wu, A. F. Koenderink, L. Torrente Murciano, M. Schwartzkopf, S. V. Roth, P. Müller-Buschbaum, J. J. Baumberg, S. D. Stranks, N. C. Greenham, L. Polavarapu, W. Zhang, A. Rao, R. L. Z. Hoye, *Nat. Photonics* **2024**, *18*, 586.

[22] S. Kumar, T. Marcato, F. Krumeich, Y.-T. Li, Y.-C. Chiu, C.-J. Shih, *Nat. Commun.* **2022**, *13*, 2106.

[23] Y. Zou, Q. Huang, Y. Yang, M. Ban, S. Li, Y. Han, T. Wu, Y. Tan, X. Gao, T. Song, B. Sun, *Adv. Mater. Interfaces* **2018**, *5*, 1801030.

[24] B. Zhao, M. Vasilopoulou, A. Fakharuddin, F. Gao, A. R. Mohd Yusoff, R. H. Friend, D. Di, *Nat. Nanotechnol.* **2023**, *18*, 981.

[25] M. Xie, Y. Zhu, R. Wang, J. Tian, *J. Phys. Chem. Lett.* **2021**, *12*, 10735.

[26] Y. Hassan, J. H. Park, M. L. Crawford, A. Sadhanala, J. Lee, J. C. Sadighian, E. Mosconi, R. Shivanna, E. Radicchi, M. Jeong, C. Yang, H. Choi, S. H. Park, M. H. Song, F. De Angelis, C. Y. Wong, R. H. Friend, B. R. Lee, H. J. Snaith, *Nature* **2021**, *591*, 72.

[27] J.-N. Yang, Y. Song, J.-S. Yao, K.-H. Wang, J.-J. Wang, B.-S. Zhu, M.-M. Yao, S. U. Rahman, Y.-F. Lan, F.-J. Fan, H.-B. Yao, *J. Am. Chem. Soc.* **2020**, *142*, 2956.

[28] Y. Hassan, O. J. Ashton, J. H. Park, G. Li, N. Sakai, B. Wenger, A.-A. Haghighirad, N. K. Noel, M. H. Song, B. R. Lee, R. H. Friend, H. J. Snaith, *J. Am. Chem. Soc.* **2019**, *141*, 1269.

[29] A. J. Knight, A. D. Wright, J. B. Patel, D. P. McMeekin, H. J. Snaith, M. B. Johnston, L. M. Herz, *ACS Energy Lett.* **2019**, *4*, 75.

[30] W. Mao, C. R. Hall, S. Bernardi, Y.-B. Cheng, A. Widmer-Cooper, T. A. Smith, U. Bach, *Nat. Mater.* **2021**, *20*, 55.

[31] A. J. Knight, L. M. Herz, *Energy Environ. Sci.* **2020**, *13*, 2024.

[32] P. Vashishtha, J. E. Halpert, *Chem. Mater.* **2017**, *29*, 5965.

[33] W. J. Mir, A. Alamoudi, J. Yin, K. E. Yorov, P. Maity, R. Naphade, B. Shao, J. Wang, M. N. Lintangpradipto, S. Nematulloev, A.-H. Emwas, A. Genovese, O. F. Mohammed, O. M. Bakr, *J. Am. Chem. Soc.* **2022**, *144*, 13302.

[34] M. Xie, J. Guo, X. Zhang, C. Bi, L. Zhang, Z. Chu, W. Zheng, J. You, J. Tian, *Nano Lett.* **2022**, *22*, 8266.

[35] C. Xie, A. Zhang, L. Chen, P. Yang, *ACS Appl. Nano Mater.* **2022**, *5*, 12552.

[36] Y.-K. Wang, F. Yuan, Y. Dong, J.-Y. Li, A. Johnston, B. Chen, M. I. Saidaminov, C. Zhou, X. Zheng, Y. Hou, K. Bertens, H. Ebe, D. Ma, Z. Deng, S. Yuan, R. Chen, L. K. Sagar, J. Liu, J. Fan, P. Li, X. Li, Y. Gao, M.-K. Fung, Z.-H. Lu, O. M. Bakr, L.-S. Liao, E. H. Sargent, *Angew. Chem., Int. Ed.* **2021**, *60*, 16164.

[37] Y.-F. Lan, J.-S. Yao, J.-N. Yang, Y.-H. Song, X.-C. Ru, Q. Zhang, L.-Z. Feng, T. Chen, K.-H. Song, H.-B. Yao, *Nano Lett.* **2021**, *21*, 8756.

[38] J.-K. Sun, S. Huang, X.-Z. Liu, Q. Xu, Q.-H. Zhang, W.-J. Jiang, D.-J. Xue, J.-C. Xu, J.-Y. Ma, J. Ding, Q.-Q. Ge, L. Gu, X.-H. Fang, H.-Z. Zhong, J.-S. Hu, L.-J. Wan, *J. Am. Chem. Soc.* **2018**, *140*, 11705.

[39] A. Dutta, S. K. Dutta, S. Das Adhikari, N. Pradhan, *Angew. Chem., Int. Ed.* **2018**, *57*, 9083.

[40] J. A. Steele, H. Jin, I. Dovgaliuk, R. F. Berger, T. Braeckevelt, H. Yuan, C. Martin, E. Solano, K. Lejaeghere, S. M. J. Rogge, C. Notebaert, W. Vandezande, K. P. F. Janssen, B. Goderis, E. Debroye, Y.-K. Wang, Y. Dong, D. Ma, M. Saidaminov, H. Tan, Z. Lu, V. Dyadkin, D. Chernyshov, V. Van Speybroeck, E. H. Sargent, J. Hofkens, M. B. J. Roeffaers, *Science* **2019**, *365*, 679.

[41] A. Ghorai, S. Mahato, S. Singh, S. Bose, B. Roy, U. Jeong, S. Kumar Ray, *Angew. Chem., Int. Ed.* **2023**, *62*, 202302852.

[42] S. Masi, A. F. Gualdrón-Reyes, I. Mora-Seró, *ACS Energy Lett.* **2020**, *5*, 1974.

[43] B. Wang, N. Novendra, A. Navrotsky, *J. Am. Chem. Soc.* **2019**, *141*, 14501.

[44] A. Marronnier, G. Roma, S. Boyer-Richard, L. Pedesseau, J.-M. Jancu, Y. Bonnassieux, C. Katan, C. C. Stoumpos, M. G. Kanatzidis, J. Even, *ACS Nano* **2018**, *12*, 3477.

[45] F. Ke, C. Wang, C. Jia, N. R. Wolf, J. Yan, S. Niu, T. P. Devereaux, H. I. Karunadasa, W. L. Mao, Y. Lin, *Nat. Commun.* **2021**, *12*, 461.

[46] D. B. Straus, S. Guo, R. J. Cava, *J. Am. Chem. Soc.* **2019**, *141*, 11435.

[47] R. J. Sutton, M. R. Filip, A. A. Haghighirad, N. Sakai, B. Wenger, F. Giustino, H. J. Snaith, *ACS Energy Lett.* **2018**, *3*, 1787.

[48] K. Wang, Z. Jin, L. Liang, H. Bian, D. Bai, H. Wang, J. Zhang, Q. Wang, S. Liu, *Nat. Commun.* **2018**, *9*, 4544.

[49] C. Wang, W. Meng, Y. Li, G. Xu, M. Peng, S. Nie, Z. Deng, *Nanoscale* **2023**, *15*, 1661.

[50] H. Huang, Y. Li, Y. Tong, E.-P. Yao, M. W. Feil, A. F. Richter, M. Döblinger, A. L. Rogach, J. Feldmann, L. Polavarapu, *Angew. Chem., Int. Ed.* **2019**, *58*, 16558.

[51] H. M. Lai, Z. Lu, C. K. K. Choi, W. Zhou, C. Ngo Yau, B. Z. Tang, H. Ko, *ACS Appl. Nano Mater.* **2022**, *5*, 12366.

[52] M. Lu, X. Zhang, Y. Zhang, J. Guo, X. Shen, W. W. Yu, A. L. Rogach, *Adv. Mater.* **2018**, *30*, 1804691.

**ADVANCED
SCIENCE NEWS**

www.advancedsciencenews.com

**ADVANCED
OPTICAL
MATERIALS**

www.advopticalmat.de

[53] S. Liu, Y. Chen, Y. Zhao, W. Xiang, X. Liang, *Mater. Lett.* **2020**, *259*, 126857.

[54] L. Yang, J. Huang, Z. Xu, Y. Li, S. Hou, Y. Tan, J. Du, X. Wang, Z. Li, A. Pan, *Adv. Opt. Mater.* **2023**, *11*, 2202561.

[55] W. Shen, Y. Dai, B. Cai, S. Chen, H. Yang, Y. Ma, Y. Chen, Z. Su, J. Zhang, Y. Qiu, Y. Wang, J. Jiang, L. Liu, K. Cao, S. Chen, *ACS Energy Lett.* **2023**, *8*, 2561.

[56] X. Huang, J. Hu, C. Bi, J. Yuan, Y. Lu, M. Sui, J. Tian, *Chem. Eng. J.* **2021**, *421*, 127822.

[57] J. Shamsi, A. S. Urban, M. Imran, L. De Trizio, L. Manna, *Chem. Rev.* **2019**, *119*, 3296.

[58] F. Krieg, Q. K. Ong, M. Burian, G. Rainò, D. Naumenko, H. Amenitsch, A. Süess, M. J. Grotevent, F. Krumeich, M. I. Bodnarchuk, I. Shorubalko, F. Stellacci, M. V. Kovalenko, *J. Am. Chem. Soc.* **2019**, *141*, 19839.

[59] S. F. Solari, L.-N. Poon, M. Wörle, F. Krumeich, Y.-T. Li, Y.-C. Chiu, C.-J. Shih, *J. Am. Chem. Soc.* **2022**, *144*, 5864.

[60] G. Huang, C. Wang, S. Xu, S. Zong, J. Lu, Z. Wang, C. Lu, Y. Cui, *Adv. Mater.* **2017**, *29*, 1700095.

[61] W. van der Stam, J. J. Geuchies, T. Altantzis, K. H. W. van den Bos, J. D. Meeldijk, S. Van Aert, S. Bals, D. Vanmaekelbergh, C. de Mello Donega, *J. Am. Chem. Soc.* **2017**, *139*, 4087.

[62] Q. A. Akkerman, D. Meggiolaro, Z. Dang, F. De Angelis, L. Manna, *ACS Energy Lett.* **2017**, *2*, 2183.

[63] J. Butkus, P. Vashishtha, K. Chen, J. K. Gallaher, S. K. K. Prasad, D. Z. Metin, G. Laufersky, N. Gaston, J. E. Halpert, J. M. Hodgkiss, *Chem. Mater.* **2017**, *29*, 3644.

[64] T. Qiao, D. H. Son, *Acc. Chem. Res.* **2021**, *54*, 1399.

[65] S. Paul, S. Acharya, *ACS Energy Lett.* **2022**, *7*, 2136.

[66] X. Shen, Y. Zhang, S. V. Kershaw, T. Li, C. Wang, X. Zhang, W. Wang, D. Li, Y. Wang, M. Lu, L. Zhang, C. Sun, D. Zhao, G. Qin, X. Bai, W. W. Yu, A. L. Rogach, *Nano Lett.* **2019**, *19*, 1552.

[67] G. H. Ahmed, Y. Liu, I. Bravić, X. Ng, I. Heckelmann, P. Narayanan, M. S. Fernández, B. Monserrat, D. N. Congreve, S. Feldmann, *J. Am. Chem. Soc.* **2022**, *144*, 15862.

[68] S. Feldmann, M. K. Gangishetty, I. Bravić, T. Neumann, B. Peng, T. Winkler, R. H. Friend, B. Monserrat, D. N. Congreve, F. Deschler, *J. Am. Chem. Soc.* **2021**, *143*, 8647.

[69] P. Luo, W. Xia, S. Zhou, L. Sun, J. Cheng, C. Xu, Y. Lu, *J. Phys. Chem. Lett.* **2016**, *7*, 3603.

[70] C.-C. Lin, S.-K. Huang, C.-E. Hsu, Y.-C. Huang, C.-Y. Wei, C.-Y. Wen, S.-S. Li, C.-W. Chen, C.-C. Chen, *J. Phys. Chem. Lett.* **2020**, *11*, 3287.

[71] B. A. Koscher, J. K. Swabeck, N. D. Bronstein, A. P. Alivisatos, *J. Am. Chem. Soc.* **2017**, *139*, 6566.

[72] J. Ye, M. M. Byranvand, C. O. Martínez, R. L. Z. Hoye, M. Saliba, L. Polavarapu, *Angew. Chem., Int. Ed.* **2021**, *60*, 21636.

[73] B. J. Bohn, Y. Tong, M. Gramlich, M. L. Lai, M. Döblinger, K. Wang, R. L. Z. Hoye, P. Müller-Buschbaum, S. D. Stranks, A. S. Urban, L. Polavarapu, J. Feldmann, *Nano Lett.* **2018**, *18*, 5231.

[74] C. F. Holder, R. E. Schaak, *ACS Nano* **2019**, *13*, 7359.

[75] S. Mahato, A. Ghorai, A. Mondal, S. K. Srivastava, M. Modak, S. Das, S. K. Ray, *ACS Appl. Mater. Interfaces* **2022**, *14*, 9711.

[76] B. Roy, S. Mahato, S. Bose, A. Ghorai, S. K. Srivastava, N. C. Das, S. K. Ray, *Chem. Mater.* **2023**, *35*, 1601.

[77] C. Bi, X. Sun, X. Huang, S. Wang, J. Yuan, J. X. Wang, T. Pullerits, J. Tian, *Chem. Mater.* **2020**, *32*, 6105.

[78] Y. Dong, T. Qiao, D. Kim, D. Rossi, S. J. Ahn, D. H. Son, *Chem. Mater.* **2019**, *31*, 5655.

[79] J. T. DuBose, A. Christy, J. Chakkamalayath, P. V. Kamat, *ACS Mater. Lett.* **2021**, *4*, 93.

[80] N. Pradhan, *Acc. Chem. Res.* **2021**, *54*, 1200.

[81] X. Zheng, Y. Hou, H.-T. Sun, O. F. Mohammed, E. H. Sargent, O. M. Bakr, *J. Phys. Chem. Lett.* **2019**, *10*, 2629.

[82] P. Liu, W. Chen, W. Wang, B. Xu, D. Wu, J. Hao, W. Cao, F. Fang, Y. Li, Y. Zeng, R. Pan, S. Chen, W. Cao, X. W. Sun, K. Wang, *Chem. Mater.* **2017**, *29*, 5168.

[83] K. Hoshi, T. Chiba, J. Sato, Y. Hayashi, Y. Takahashi, H. Ebe, S. Ohisa, J. Kido, *ACS Appl. Mater. Interfaces* **2018**, *10*, 24607.

[84] V. M. Goldschmidt, *Naturwissenschaften* **1926**, *14*, 477.

[85] R. D. Shannon, *Acta Crystallogr. A* **1976**, *32*, 751.

[86] G. Greczynski, L. Hultman, *Sci. Rep.* **2021**, *11*, 11195.

[87] A. Wieczorek, H. Lai, J. Pious, F. Fu, S. Siol, *Adv. Mater. Interfaces* **2023**, *10*, 2201828.

[88] K. N. Wood, G. Teeter, *ACS Appl. Energy Mater.* **2018**, *1*, 4493.

[89] T. Liu, X. Zhao, J. Li, Z. Liu, F. Liscio, S. Milita, B. C. Schroeder, O. Fenwick, *Nat. Commun.* **2019**, *10*, 5750.

[90] D. N. Dirin, A. Vivani, M. Zacharias, T. V. Sekh, I. Cherniukh, S. Yakunin, F. Bertolotti, M. Aebli, R. D. Schaller, A. Wieczorek, S. Siol, C. Cancellieri, L. P. H. Jeurgens, N. Masciocchi, A. Guagliardi, L. Pedesseau, J. Even, M. V. Kovalenko, M. I. Bodnarchuk, *Nano Lett.* **2023**, *23*, 1914.

[91] S. Siol, J. Mann, J. Newman, T. Miyayama, K. Watanabe, P. Schmutz, C. Cancellieri, L. P. H. Jeurgens, *Surf. Interface Anal.* **2020**, *52*, 802.

[92] S. Zhuk, S. Siol, *Appl. Surf. Sci.* **2022**, *601*, 154172.

[93] A. S. Gorzalski, C. Donley, O. Coronell, *J. Membr. Sci.* **2017**, *522*, 31.

[94] A. T. Appapillai, A. N. Mansour, J. Cho, Y. Shao-Horn, *Chem. Mater.* **2007**, *19*, 5748.

[95] J. A. Vigil, B. M. Wieliczka, B. W. Larson, M. Abdelsamie, N. S. Dutta, M. A. Haque, A. Hazarika, J. M. Luther, M. F. Toney, *Chem. Mater.* **2023**, *35*, 9924.

[96] C. J. Krajewska, A. E. K. Kaplan, M. Kick, D. B. Berkinsky, H. Zhu, T. Sverko, T. Van Voorhis, M. G. Bawendi, *Nano Lett.* **2023**, *23*, 2148.

[97] J. A. Schuller, S. Karaveli, T. Schiros, K. He, S. Yang, I. Kymissis, J. Shan, R. Zia, *Nat. Nanotechnol.* **2013**, *8*, 271.